Analysis and Design of Surface Permanent Magnet Synchronous Motor and Generator

Chengyuan He, *Member, IEEE*, and Thomas Wu, *Senior Member, IEEE*

***Abstract*— This paper presents an analytical method to design the high-efficiency surface permanent magnet synchronous motor (SPMSM) or generator (SPMSG). The air-gap and permanent magnet size can be approximately determined based on our mathematics model, which is the most important part of SPMSM design. From our method, we can know that motor's power out torque is related to the torque angle that we selected in our design and it affects the air-gap and permanent magnet size. If we choose a low torque angle, the motor or generator's overload power handing capability will increase. The embrace value has a vital place in designing a motor or generator due to its effects on air gap flux density, cogging torque, efficiency and so on. In order to avoid the knee effect, the working point of the permanent magnet we selected in the design should be bigger than 0.5. The developed 36 slots, 4 poles, surface mound permanent generator is proposed. The corresponding finite element analysis (FEA) model is built based on our design method. Structure optimization includes stator and rotor structure size, permanent magnet size, magnetic bridge and air gap length which are analyzed and simulated by ANSYS Maxwell 2D FEA. Thermal analysis is conducted, and the housing of the alternator is designed. The alternator prototype is fabricated and tested based on our design.**

***Index Terms*—Finite element analysis; fabrication, high-efficiency, mathematic model, surface permanent magnet synchronous motor or generator.**

I. INTRODUCTION

SURFACE permanent magnet synchronous motor or generator is widely used in industrial application such as an auxiliary power unit, robotic arms, electrical tools and so on due to its high power density [1]-[5]. For SPMSM or SPMSG, the direct- and quadrature-axes inductances are the same. There is essentially no reluctance torque generated by SPM motor. The flux leakage of them are few, which make the design easier compared with interior permanent magnet machines [6] [7] [8]. We can give an approximate flux leakage in the design. The most important part of the design is to determine the air-gap and permanent magnet thickness [9] [10][11]. We provide the mathematic model to get the initial parameters of SPMSM or SPMSG. Then we can use Maxwell 2D FEM to optimize all the initial design parameter, which will give a guidance for the SPMSM or SPMSG design. Our mathematic model has three important factors (permanent magnet working point, permanent magnet embrace, and torque angle). These three factors are related to the air-gap size, permanent magnet size, efficiency, cogging torque and over- load capacity. We can see the detailed relationship between them in our design equations.

The working point of a permanent magnet should be selected when doing the design. The maximum power is reached when the working point of permanent is 0.5. In order to avoid demagnetization of the magnet [12] [13] [14], The working point should be selected higher than 0.5. The design can utilize a smaller torque angle to get high overload capacity [15] [16], which will increase the magnet thickness and air-gap size. The magnet embrace [17] [18] affects the cogging torque and efficiency. After we selected the working point of permanent magnet and torque angle, the permanent magnet thickness and air-gap size are also related to the value of magnet embrace. A 2kW, 6000 rpm generator was designed and fabricated based on our design method. Copper loss [19] [20] is the most significant of all the losses in low and medium speed electric machines. Reducing the copper loss is the key to build highly-efficiency machine. Lower current density copper wires that have large wire cross section is selected in the generator design, which will significantly reduce the copper loss. It also makes thermal management easier and avoids using active cooling methodologies (such as fan, liquid cooling or spray cooling).

This paper is organized in the following sections: section II focuses on the motor key design points. Section III then looks at the analysis of the mathematic model. Section IV and V proceeds to show the designed generator Maxwell model and associated simulation analysis as well as thermal analyze. Generator prototype and testing are shown in section VI.

II. GUIDELINES

For the SPMSM or SPMSG design, it is necessary to determine the stator and rotor size, number of slots and poles, number of winding turns, air-gap and magnet thickness. Stator and rotor preliminary size can be obtained from the design equation. Numbers of slots and poles [21] [22] are based on two factors: the greatest common divider (GCD) between the slot

Manuscript was submitted for review on 02, May, 2018

Chengyuan He is with the Department of Electrical and Computer Engineering, University of Central Florida, Orlando, Fl, 32816 USA e-mail: (ChengyuanHe@knights.ucf.edu).

Thomas Wu is with the Department of Electrical and Computer Engineering, University of Central Florida, Orlando, Fl, 32816 USA e-mail: (Thomas.Wu@ucf.edu).

Digital Object Identifier 10.30941/CESTEMS.2019.00013

and pole number, and the least common multiplier (LCM) between the slot number and the pole number. The number of winding turns is related to the phase current the cooling methods. For the magnet material [23] [24], NdFeB and SmCo are the two most popular materials. NdFeB is the strongest rare-earth material, but the curie and operating temperature of NdFeB are slow. SmCo is the second strongest material with much higher Curie operating temperature range, but its price is expensive. All these are the basic design part. A much smaller torque angle δ than that in traditional design at relating load is used, which is between about 2 degrees and about 10 degrees. It results in large air-gap and large magnet thickness. The larger air-gap helps to reduce the windage loss and noise level, while the increased magnet thickness contributes to avoiding demagnetization. The relationship among the torque angle δ, working point, and the permanent magnet embrace will be analyzed. The key design part of SPMSM or SPMSG is how to determine the magnet thickness and air-gap size. The corresponding magnet thickness and air-gap size based on the much smaller torque angle will be determined according to the design method. The following section will focus on the key design part.

A. Working point of Permanent Magnet

For a multi-pole surface mount rotor as shown in Fig. 1, according to the magnetic circuit analysis, we get:

$$2H_g g + 2H_m d_m = 0 \tag{1}$$

where H_g is the air gap magnetic field intensity, g is the air gap size, H_m is the PM magnetic field intensity and dm is the magnetic thickness. Using magnetic flux density B to replace magnetic filed intensity H, then the (1) can be expressed as:

$$\frac{d_m}{g} = -\frac{B_m}{\mu_0 H_m}\frac{A_m}{A_g} \tag{2}$$

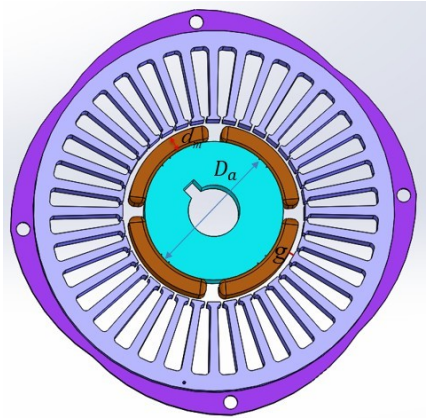

Fig. 1. Rotor with multi-pole surface-mounted magnets

The relationship between magnet thickness and air-gap is obviously from (2). It is a key procedure of choosing a working point for the permanent magnet when determining the size of the permanent magnet and air-gap.

Firstly, maximum energy point will be determined. B can be got from Fig. 2 easily:

$$B = \frac{B_r}{H_c}(H + H_c), \tag{3}$$

letting B multiply H, then BH can be expressed as:

$$BH = \frac{B_r}{H_c}(H + H_c)H, \tag{4}$$

maximum energy point can be obtained through BH derivative:

$$\frac{\partial(BH)}{\partial H} = 0 \tag{5}$$

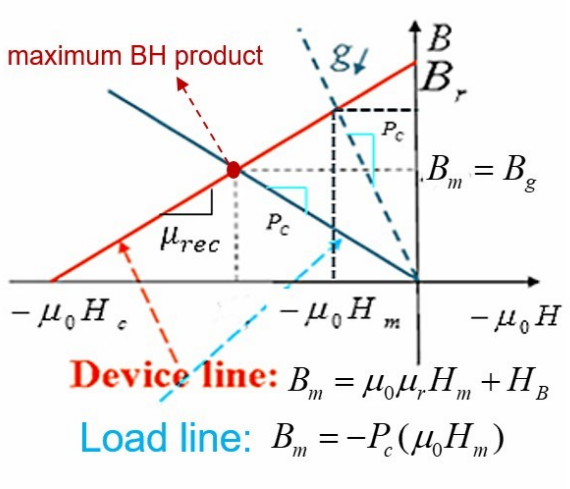

Fig. 2. B-H curve of a permanent magnet material

After some derivation, it can be known that $(BH)_{\max}$ located in $B_m = B_r/2, H_m = -H_c/2$, which is in the middle of device line. It can be seen that there are two lines in Fig. 2: device line and load line. The device line is defined as the theoretical demagnetization cure and load line is the line through the origin to the working point. Device line equation can be easily obtained:

$$B_m = (\frac{B_r}{H_c})(H_m + H_c) = \mu_0\mu_r H_m + H_B \tag{6}$$

P_c is called pemeance coefficient, which is equal to:

$$P_c = \frac{d_m}{g}\frac{A_g}{A_m} = \frac{A_g/g}{A_m/d_m} \approx \frac{R_m}{R_g}. \tag{7}$$

From the magnetic circuit, it is obvious that:

$$F_m + F_g = 0, \tag{8}$$

where $F_m = H_m d_m$, and $F_g = H_g g$. Putting them to (8), then $H_g = -\frac{d_m}{g}H_m$ can be obtained. Finally, B_g can be expressed as:

$$B_m = -\mu_0\frac{d_m}{g}\frac{A_g}{A_m}H_m = -P_c(\mu_0 H_m). \tag{9}$$

Defining $B_m = -\mu_0\frac{d_m}{g}\frac{A_g}{A_m}, H_m = -P_c(\mu_0 H_m)$, where α_m is called working point of a permanent magnet. The maximum energy can be reached by choosing α = 0.5. However, in order to avoid demagnetization and knee effect, working point is always chosen higher than 0.5.

B. The Air-gag Magnetic Flux Density From PM Rotor

Air-gap Magnetic flux density from PM rotor affects the air-gap peak flux density value and peak winding magnetic

density. Parallel magnetization is widely used in SPMSM or SPMSG.

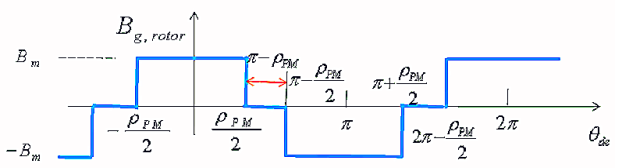

Fig. 3. The parallel magnetization waveform

Fig. 3 shows the parallel magnetization waveform, after doing Fourier expansion, the air-gap magnetic flux density can be expressed as:

$$B_{rh}=\frac{2}{2\pi}[\int_{-\rho_{PM/2}}^{\rho_{PM/2}}B_m\cos(h\theta_{ae})d\theta_{ae}+\int_{\pi-\rho_{PM/2}}^{\pi+\rho_{PM/2}}-B_m\cos(h\theta_{ae})d\theta_{ae}]=\frac{4}{\pi}\frac{\sin(h\frac{\rho_{PM}}{2})}{h}B_m \quad (11)$$

where ρ_{PM} is the electrical angle of permanent magnet, can be calculated by $\rho_{PM}=e_m\pi$, where e_m represents the embrace of the permanent magnet. Its value varies from 0.5 to 1. It affects the air-gap magnetic field, peak flux density of the teeth and yoke, cogging torque, etc, k_{ph} is pitch factor for the h^{th} harmonic, $k_{ph}=\sin(h\rho_{PM}/2)B_m$. The peak air-gap magnetic flux density $B_{r,pk}$ can be approximately calculated by:

$$B_{r,pk}\approx\frac{4}{\pi}\sin(\frac{\rho_{PM}}{2})B_m. \quad (12)$$

Typically, power angle θ of surface permanent magnet motor is approximately to 0 at full-load. The phase diagram is shown in Fig. 4.

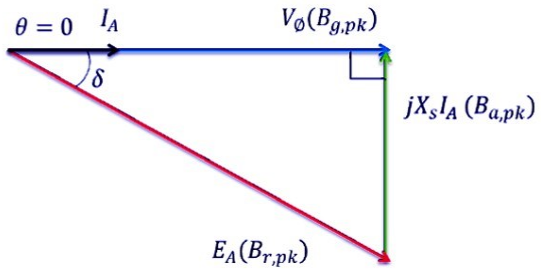

Fig. 4. The phase diagram when the θ = 0

The torque angle δ for SPMSM or SPMSG is usually designed to be in the range of 15-30 degree. In order to get more power handling capability and pull out torque, a lower torque angle should be selected in the design. The peak value of the net magnetic flux density $B_{g,pk}$ and peak winding magnetic flux density $B_{a,pk}$ are defined:

$$B_{g,pk}=B_{r,pk}\cos\delta, B_{a,pk}=B_{r,pk}\sin\delta. \quad (13)$$

C. Magnet Thickness and Air-gap Size

Normally the air-gap of low and medium power SPMSM or SPMSG is small. The peak winding magnetic flux density can be calculated as:

$$B_{a,peak}=\frac{4}{\pi}\frac{\mu_0}{\hat{g}_{toatal}}\frac{\hat{N}_a}{P}1.5\sqrt{2}I_{A,rated}, \quad (14)$$

And the initial total effective air-gap size can be obtained based on (14)

$$\hat{g}_{total}=\frac{4}{\pi}\frac{\mu_0}{g_{a,peak}}\frac{\hat{N}_a}{P}1.5\sqrt{2}I_{A,rated}, \quad (15)$$

where $$\hat{g}_{total}=k_c g'_{total}, \quad (16)$$

where k_c is called cater's coefficient and can be approximately determined by:

$$k_c\approx\frac{\tau_s}{\tau_s-\frac{b_{s0}^2}{5g'_{total}+b_{s0}}}, \quad (17)$$

where $g'_{total}=g+d_m/\mu_{rm}$. It is known that $d_m/g\approx P_c$ and $P_c=\frac{\alpha_m}{1-\alpha_m}\mu_{rm}$, after some derivation, the air-gap size can be determined by:

$$g=(1-\alpha_m)g'_{total}d_m=\alpha_m g'_{total}\mu_{rm} \quad (18)$$

If the designed air gap is large, it is necessary to calculated the Magnet motive Force (MMF) from the permanent magnet and MMF generated from the air gap. The total MMF from the two parts can be added up and expressed by:

$$F_{total}=\frac{r_g B_{r,pk}}{\mu_0}\left[\frac{1}{\mu_{rm}}\ln(\frac{r_a+d_m}{r_a})+\ln(\frac{r'_{is}}{r_a+d_m})\right], \quad (19)$$

where $r'_{is}=r_a+d_m+g_{eff}$, r_g is the radius of the actual air gap, r_a represents the inner radius of the rotor. According (19), g_{eff} can be obtained, then, the actual air gap and magnet thickness can be obtained.

III. Analysis of Mathematic Model

From magnet thickness and air-gap equation, we can know that air-gap magnetic flux density value B_{rh} is a key design factor. The working point of a permanent magnet, permanent magnet embrace value affects the value of B_{rh}. The torque angle δ determines the peak value of the net magnetic flux density and the peak winding magnetic flux density and it is also related to the pull-out torque and over-load capacity. The smaller the torque angle, the higher the pull-out torque and over-load capacity. The permanent magnet embrace is also related to the cogging torque and efficiency. After selecting the values of the working point and torque angle, the permanent magnet embrace will play a role in the design. Normally we selected the value of magnet embrace is around 0.8. Fig. 5 and Fig. 6 show how the embrace affects the magnet thickness, air-gap values. The plots are based on a 2Kw, 6000rpm generator with 0.8 working point and selected 10-degree torque

angle. We can see that when the value of embrace increase the magnet thickness and air-gap thickness values decrease because the increased embraced value will increase the $B_{a,pk}$ and $B_{g,pk}$ values, which can be shown from (12) and (13).

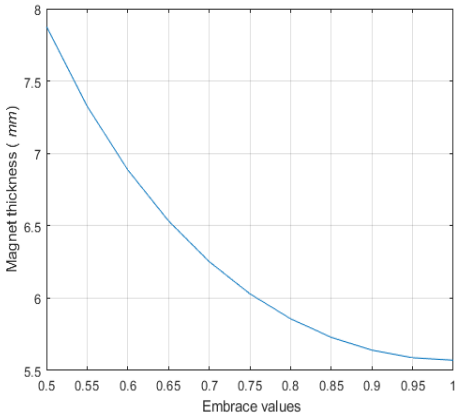

Fig. 5. Embrace values Vs Magnet thickness values.

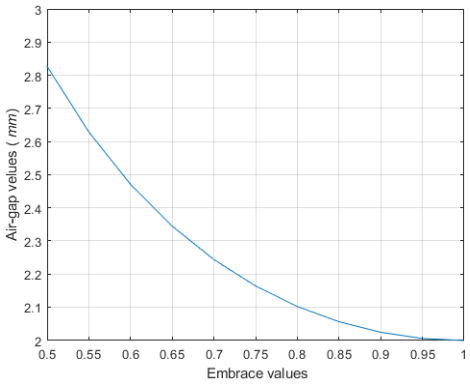

Fig. 6. Embrace values Vs air-gap values.

IV. Generator Model

A generator with 0.8 working point, 10-degree torque angle, and 0.75 embrace value was designed and fabricated based on the design method. The magnet thickness value is selected to be 6*mm*, and air-gap length is chosen to be 2*mm* after the optimization. The air-gap thickness is slightly less than the simulation value 2.15*mm* considering the fabrication process. After the analysis, the dimensions of the alternator are obtained as shown in Table I.

TABLE I
RESULTS OF THE ALTERNATOR DESIGN

Parameters	Unit	Specification
Magnetic material	-	NdFeB-38
Cool method	-	air
Rated Power	kW	2
Number of magnet poles	-	4
Number of stator slots	-	36
Stator outer diameter	mm	157
Stator inner diameter	mm	79
Airgap length	mm	2
Magnet width	mm	6
Magnet length	mm	23

ANSYS Maxwell 2D is used to evaluate and optimize the design. Parameters such as slot size and shape, magnet thickness, air-gap size and yoke thickness, and so on have been optimized using the software. Fig.7 shows the distribution of magnetic flux density. It shows that the tooth flux density is limited to 1.1T and the maximum flux density of the yoke is around 1.45T. Fig. 8 shows the calculated efficiency of the alternator versus RMS phase current. It can be seen that the motor has a very high efficiency (around 97%) at the rated power.

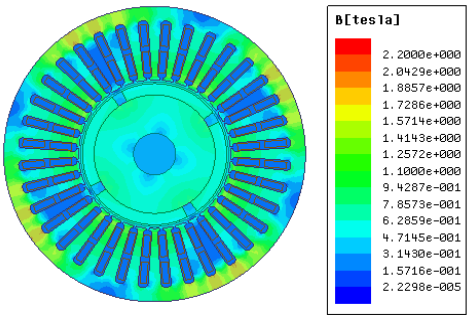

Fig. 7. Flux density in the generator.

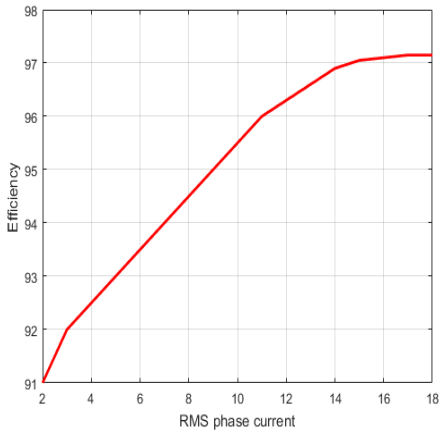

Fig. 8. Efficiency vs. RMS phase current.

Fig. 9 shows flux linkage is good sinusoidal shape, which indicates the magnetic does not saturate with high excitation. Thus, the distortion of EMF should not appear across the zero point. Besides the amplitude of A, B and C phases flux linkage are almost the same, which can be explained as that the fringing effect is minimal. Fig. 10 shows the cogging torque versus time. It shows that the cogging torque is low. The cogging torque peak value is around 0.015 N.

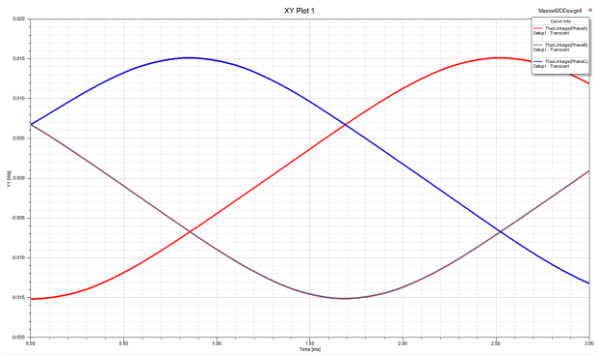

Fig. 9. Phase flux Vs time.

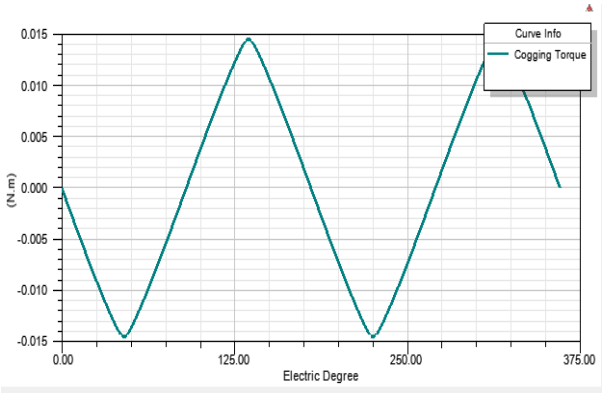

Fig. 10. Cogging torque Vs electric angle.

The flux density of the air-gap and no-load air-gap flux density four transform analysis are shown in Fig. 11. It indicates that the even harmonics are canceled, only odd harmonics exist.

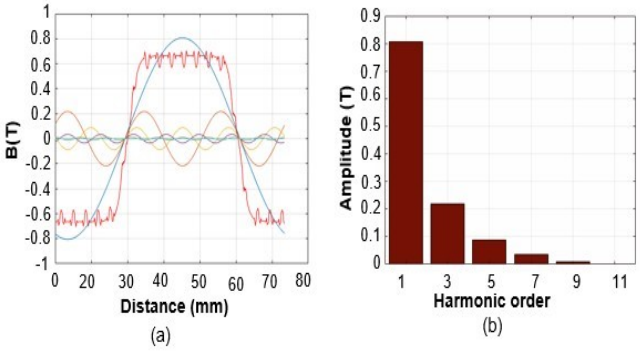

Fig. 11. (a) The flux density of air-gap and different order harmonic waveforms showing with different color; (b) The fast Fourier transformation (FFT) analysis of air-gap.

V. Thermal Analyze

The housing is designed and the thermal performance of each part of the generator are analyzed as shown in Fig. 12. The peak temperature inside the generator is around 342K at the full load, which is below 350K and therefore the active cooling methodologies are not needed.

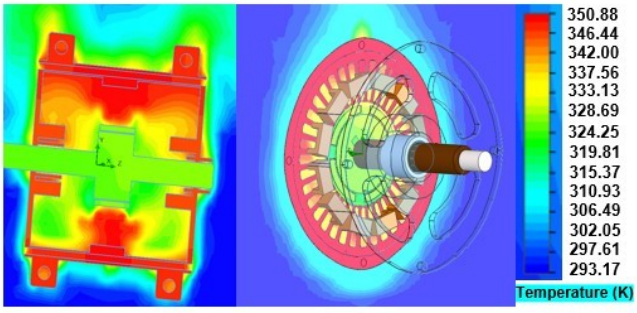

Fig. 12. The simulation of generator temperature of each parts

VI. Motor Prototype And Testing

The alternator prototypes are shown in Fig. 13. We use lamination technique to reduce the core loss. The lamination factor is 0.92.

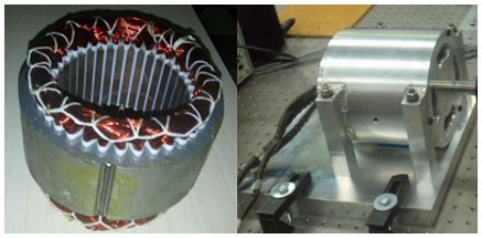

Fig. 13. Generator prototype.

Fig. 14 shows the testing set. A permanent magnet motor is used to drive the alternator. The resistors are worked as load and connected to the generator three phase outputs. We can see the three phase currents in Fig. 15. The waveforms are not perfect sine wave due to harmonics. Finally, the efficiency of the alternator under different loads has been tested as shown in Fig. 16, which indicates the design of alternator has high efficiency. The efficiency is around 95 % at the rated load, which is 2% lower than the simulation values. Because when we do the simulation, we ignore some factors effect.

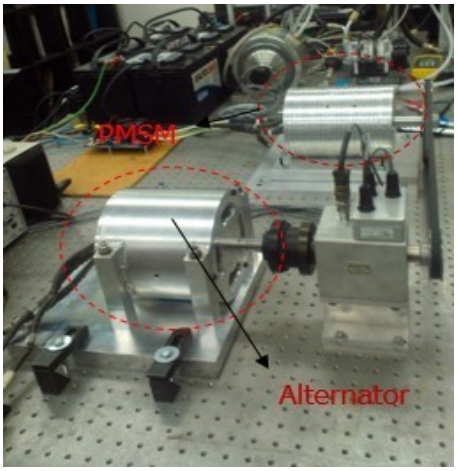

Fig. 14. Generator system testing set.

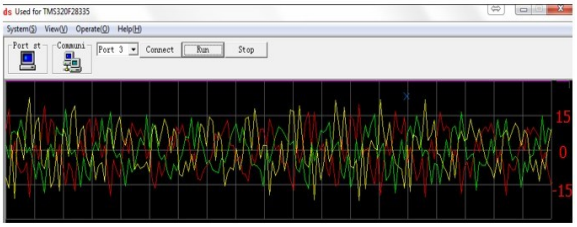

Fig. 15. Generator three phase current.

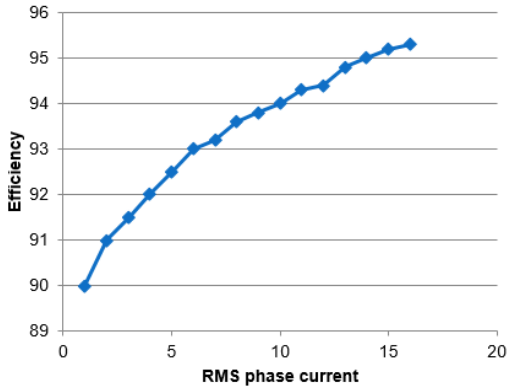

Fig. 16. Three phase RMS current vs efficiency.

VII. CONCLUSION

An analytical method to design the high- efficiency surface permanent magnet synchronous motor or generator was introduced. The machinery's magnetic thickness and air-gap size can be obtained through the method. How the air-gap magnetic flux density value, working point of a permanent magnet, torque angle and the magnet embrace effect the magnet thickness and air-gap size was also analyzed. A 2 kW 6000 rpm surface-mounted permanent magnets generator with 36-slot, ,4-pole topology was been successfully designed. The design has been optimized and verified using MAXWELL 2D analysis based on the finite element method. The housing is designed and the thermal performance of each part to the generator are analyzed. The heat dissipation performance of our generator is pretty good, and no fan is required in our design. The generator has also been completely fabricated. The simulation and test results show the key characteristics and performance of the alternator are met. The future research of this generator application will focus on the sensor-less control system design. Three phase active rectifier will be designed to get DC bus voltage from three phase outputs of generator.

REFERENCES

[1] Li Yu, Zhuoran Zhang, Zhihui Chen, and Yangguang Yan, "Analysis and Verification of the Doubly Salient Brushless DC Generator for Automobile Auxiliary Power Unit Application," *IEEE Transactions on Industrial Electronics,* vol. 61, no. 12, pp.6655,6663, Dec. 2014.

[2] Do-Kwan Hong, Wook Hwang, Ji-Young Lee and Byung-Chul Woo,"Design, Analysis, and Experimental Validation of a Permanent Magnet Synchronous Motor for Articulated Robot Applications," *IEEE Transaction on Magnetics,* vol. 54, no. 3, March 2018.

[3] Chengyuan He and Thomas Wu, "Permanent Magnet Brushless DC Motor and Mechanical Structure Design for the Electric Impact Wrench System," *Energies,* vol. 11, no. 6, pp. 1360, 2018.

[4] Ankita Dwivedi, Santosh Kumar Singh, Rakesh K. Srivastava and Som N. Mahendra, "Comparative study and performance evaluation of analytical methods for surface mounted permanent magnet brushless motors," *IET Power Electronics,* vol. 9, pp. 2289-2297, 15 September 2016.

[5] Feng Liang, J. M. Miller and Xingyu Xu, "A vehicle electric power generation system with improved output power and efficiency," *IEEE Transactions on Industry Applications*, Vol. 35, pp. 1341-1346, 1999.

[6] Chengyuan He and Thomas Wu, "Design and analysis of a V-type fractional-slots IPMSM with distributed winding for electric vehicles," *XXII Internatinal Conference on Electrical Machines (ICEM),* pp. 1459-1465, 2016.

[7] Chengyuan He and Thomas Wu, "Design, analysis and experiment of a permanent magnet brushless DC motor for electric impact wrench," *XXII International Conference on Electrical Machines (ICEM),* pp. 1591-1597, 2016.

[8] Jianning Dong, Yunkai Huang, Long Jin, Heyun Lin, "Comparative Study of Surface-Mounted and Interior Permanent-Magnet Motors for High-Speed Applications," *IEEE Trans on applied superconductivity,* vol. 26, no. 4, June 2016.

[9] Vansompel, Hendrik and Sergeant, Peter and Dupre´, Luc and Van den Bossche, Alex, "Axial-flux PM machines with variable air gap," *IEEE Transactions on industrial electronics,* vol. 61, pp. 730-737, 2014.

[10] Fakam, Mathias and Hecquet, Michel and Lanfranchi, Vincent and Randria, Andry, "Design and magnetic noise reduction of the surface permanent magnet synchronous machine using complex air-gap permeance," *IEEE Transactions on Magnetics,* vol. 51, no. 4, pp. 1-9, 2015.

[11] Lei, Gang and Liu, Chengcheng and Zhu, Jianguo and Guo, Youguang, "Techniques for multilevel design optimization of permanent magnet motors," *IEEE Transactions on Energy Conversion,* vol. 30, no. 5, pp. 1574-1584, 2015.

[12] Faiz, Jawad and Nejadi-Koti, H, "Demagnetization fault indexes in permanent magnet synchronous motors—An overview," *IEEE Transactions on Magnetics,* vol. 52, no. 4, pp. 1-11, 2016.

[13] amidizadeh, Sara and Alatawneh, Natheer and Chromik, Richard R and Lowther, David A, "Comparison of different demagnetization models of permanent magnet in machines for electric vehicle application," *IEEE Transactions on Magnetics,* vol. 52, no. 5, pp. 1-4, 2016.

[14] Goktas, Taner and Zafarani, Mohsen and Akin, Bilal, "Discernment of broken magnet and static eccentricity faults in permanent magnet synchronous motors," *IEEE Transactions on Energy Conversion,* vol. 31, no. 2, pp. 578-587, 2016.

[15] Huang, Xuzhen and Tan, Qiang and Li, Liyi and Li, Jing and Qian, Zhenyu, "Winding temperature field model considering void ratio and temperature rise of a permanent-magnet synchronous motor with high current density," *IEEE Transactions on Industrial Electronics,* vol. 64, no. 3, pp. 2168-2177, 2017.

[16] Bolvashenkov, Igor and Herzog, Hans-Georg, "Degree of fault tolerance of the multi-phase traction electric motors: methodology and application," *Environment and Electrical Engineering (EEEIC), 2016 IEEE 16th In- ternational Conference on,* pp. 1-6, 2016.

[17] Ocak, C and Dalcalı, A and Çelik, E and Uygun, D, "FEA-Based Design Improvement of Small Scale BLDCMs Considering Magnet Thickness and Pole Embrace," *Int'l Journal of Computing, Communications & Instrumentation Engg,* vol. 4, no. 2, pp. 31-35, 2017.

[18] ÖZOĞ LU, YUSUF, "New magnet shape for reducing torque ripple in an outer-rotor permanent-magnet machine," *Turkish Journal of Electrical Engineering & Computer Sciences,* vol. 25, no. 5, pp. 4381-4397, 2017.

[19] Liu, Kai and Fu, Xinghe and Lin, Mingyao and Tai, Liuchen, "Ac copper losses analysis of the ironless brushless dc motor used in a flywheel energy storage system," *IEEE Transactions on Applied Superconductivity*, vol. 26, no. 7, pp. 1-5,2016.

[20] Frandsen, Tommy V and Mathe, Laszlo and Berg, Nick Ilsoe and Holm, Rasmus Koldborg and Matzen, Torben N and Rasmussen, Peter Omand and Jensen, Kasper K. "Motor integrated permanent magnet gear in a battery electrical vehicle," *IEEE Transactions on Industry Applications,* vol. 51, no. 2, pp. 1516-1525, 2015.

[21] Wu, Leilei and Qu, Ronghai and Li, Dawei and Gao, Yuting, "Influence of pole ratio and winding pole numbers on performance and optimal design parameters of surface permanent-magnet vernier machines," *IEEE Trans. Ind. Appl.*, vol. 51, no. 5, pp. 3707-3715, 2015.

[22] Zhu, Z. Q and Howe, David, "Influence of design parameters on cogging torque in permanent magnet machines," *IEEE Transactions on energy conversion,* vol. 15, no. 4, pp. 407-412, 2000.

[23] Ruoho, Sami and Kolehmainen, Jere and Ika¨heimo, Jouni and Arkkio, Antero, "Interdependence of demagnetization, loading, and temperature rise in a permanent-magnet synchronous motor," *IEEE Transactions on Magnetics,* vol. 46, no. 3, pp. 949, 2010.

[24] Kimiabeigi, Mohammad and Widmer, James D and Long, Raymond and Gao, Yi and Goss, James and Martin, Richard and Lisle, Timothy and Vizan, Jose M Soler and Michaelides, Alex and Mecrow, Barrie C, "On selection of rotor support material for a ferrite magnet spoke-type traction motor," *IEEE Transactions on Industry Applications,* vol. 52, no. 3, 00. 2224-2233, 2016.

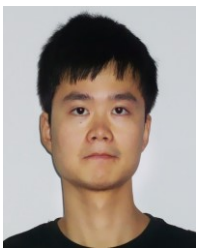

Chengyuan He was born in Yangzhou, China in 1988. He received the M.S. degree from the Wright State University of Electrical Engineering, Ohio, USA, in 2013 and Ph.D. degree in electrical engineering at the University of Central Florida, Florida, USA, in 2108. His research interests include advanced motor design and drivers, wind power technology and power electronics.

Prof. Thomas Wu received his Ph.D. degree in Electrical Engineering from the University of Pennsylvania (Penn) in 1999. In the fall of 1999, he joined the University of Central Florida (UCF) as an assistant professor. He was promoted to associate professor in 2005, and professor in 2011. He also got his tenure in 2005. Prof. Wu was ASEE Summer Faculty Fellow at Air Force Research Lab (AFRL) in the summer of 2009 and 2010. He was also appointed as the prestigious National Research Council (NRC) Senior Research Associate at AFRL from September 2010 to August 2012**.**